








## Potential roots of the deep subbarrier heavy-ion fusion hindrance phenomenon within the sudden approximation approach

P. W. Wen <sup>1,2</sup> C. J. Lin <sup>2,3,\*</sup> R. G. Nazmitdinov <sup>1,4,†</sup> S. I. Vinitzky <sup>1,5,‡</sup> O. Chuluunbaatar <sup>1,6</sup> A. A. Gusev <sup>1,4</sup>  
A. K. Nasirov,<sup>1,7</sup> H. M. Jia,<sup>2</sup> and A. Gózdź <sup>8</sup>

<sup>1</sup>Joint Institute for Nuclear Research, 141980 Dubna, Russia

<sup>2</sup>China Institute of Atomic Energy, 102413 Beijing, China

<sup>3</sup>Department of Physics, Guangxi Normal University, 541004 Guilin, China

<sup>4</sup>Dubna State University, 141982 Dubna, Russia

<sup>5</sup>Peoples' Friendship University of Russia (RUDN University), 117198 Moscow, Russia

<sup>6</sup>Institute of Mathematics and Digital Technology, Mongolian Academy of Sciences, 13330 Ulaanbaatar, Mongolia

<sup>7</sup>Institute of Nuclear Physics, Ulugbek, 100214 Tashkent, Uzbekistan

<sup>8</sup>Institute of Physics, University of M. Curie-Skłodowska, 520031 Lublin, Poland



(Received 6 December 2020; accepted 12 April 2021; published 3 May 2021)

We analyze the origin of the unexpected deep subbarrier heavy-ion fusion hindrance in  $^{64}\text{Ni} + ^{100}\text{Mo}$ ,  $^{64}\text{Ni} + ^{64}\text{Ni}$ , and  $^{28}\text{Si} + ^{64}\text{Ni}$  reactions. Our analysis is based on the improved coupled-channels description, implemented by means of the finite element method. With the aid of the Woods-Saxon potential the experimental cross sections and the  $S$  factors of these reactions are remarkably well reproduced within the sudden approximation approach. We found that accounting for the nondiagonal matrix elements of the coupling matrix, traditionally neglected in the conventional coupled-channels approaches in setting the left boundary conditions inside the potential pocket, and its minimal value are crucially important for the interpretation of experimental data. We found as well a good agreement with the general trend of the experimental data for the  $S$  factor of the fusion reaction  $^{12}\text{C} + ^{12}\text{C}$ , which has no pronounced maximum for this system.

DOI: [10.1103/PhysRevC.103.054601](https://doi.org/10.1103/PhysRevC.103.054601)

### I. INTRODUCTION

Various stages of astrophysical nucleogenesis, the synthesis of superheavy nuclei, and, consequently, effective mechanisms of nucleus-nucleus interaction [1–6] require a deep understanding of the near-barrier heavy-ion fusion reaction. Since 2002 precise measurements have been available to probe the effects of the interaction potential at deep subbarrier energies [7]. However, at these energies the fusion cross sections fall off much steeper than the conventional coupled-channels (CC) calculations predict. This fusion hindrance phenomenon is generally accompanied by the maximum of the astrophysical  $S$  factor. Due to its notable influence on the astrophysical nuclear reaction processes for fusion reactions like  $^{12}\text{C} + ^{12}\text{C}$  [8–13], this problem has been a subject of extensive studies in the past years [7,14–16].

Since the discovery of the fusion hindrance phenomenon, the consensus is that the conventional CC calculations based on a Woods-Saxon (WS) potential are insufficient to reproduce the experimental data [1,2,17]. As a result, numerous theoretical attempts have been developed to tackle this problem. Among them are the hybrid of different nuclear

potentials [18,19], the extending of the CC framework to the adiabatic states [20], the quantum diffusion approach [21], and the density-constrained frozen Hartree-Fock method [22], to name just a few.

In fact, within the conventional CC approach we can distinguish between two directions of the theoretical explanations for the hindrance mechanisms. The first one is based on the sudden approximation for a hybrid of different potentials. In particular, a gentle overlap of the reacting nuclei is considered due to the saturation properties of nuclear matter [18,23,24]. One attempt to explain the steep falloff of fusion cross sections is by using the double-folding potential with Michigan three-range Yukawa (M3Y) forces supplemented by a repulsive core. Another approach analyzes the hindrance phenomenon by fitting the fusion excitation function with two separate WS potentials [19]. On different sides of the threshold energy where the maximum of the  $S$ -factor is located, the model includes the potentials that produce a different logarithmic slope of the excitation functions.

The second direction is based on the adiabatic approximation [20,25]. On top of the conventional CC method, an extra one-dimensional adiabatic potential barrier is assumed after the reacting nuclei contact each other, which is considered the formation of the composite system. Thus, the mechanism of the deep subbarrier hindrance is still debatable. In spite of numerous attempts it remains a real challenge for nuclear reaction theory. The main goal of the present paper

\*Corresponding author: [cjlin@ciae.ac.cn](mailto:cjlin@ciae.ac.cn)

†Corresponding author: [rashid@theor.jinr.ru](mailto:rashid@theor.jinr.ru)

‡Corresponding author: [vinitzky@theor.jinr.ru](mailto:vinitzky@theor.jinr.ru)

is to explain the unexpected deep subbarrier heavy-ion fusion hindrance, providing the principle of bounding solutions for the scattering problem of two colliding nuclei, developed in Refs. [26,27].

## II. THEORETICAL FRAMEWORK

We consider the collision between two nuclei, whose relative motion is coupled to nuclear intrinsic motion. The potential between the projectile and the target contains the Coulomb potential and nuclear potential, chosen in the WS form  $V_N^{(0)}(r) = -V_0/(1 + \exp[(r - R_0)/a_0])$ . Here, the parameters  $V_0$ ,  $R_0$ , and  $a_0$  are the potential depth, potential radius, and diffuseness, respectively;  $r$  is the distance between the mass centers of the two interacting nuclei.

Following Refs. [28,29], in our approach the nuclear coupling Hamiltonian is generated by changing the target radius in the potential to the dynamical operator  $R_0 + \hat{O}$ , which is related to collective vibrations. The solution of the CC equations between values  $r_{\max}$  and  $r_{\min}$  is found under the incoming wave boundary conditions (IWBCs); i.e., a strong absorption inside the potential pocket is assumed. The right boundary point  $r_{\max}$  is usually set at a large enough distance where the interaction is weak, and the off-diagonal elements of the coupling matrix tend to be zero. The  $r_{\min}$  is determined at the minimum of the potential pocket  $V_p$ .

At the left boundary  $r = r_{\min}$ , the open left exit channel wave functions are usually taken as the plane wave  $\psi_{n_0}^{(\ell)}(r) = \exp(-ik_n(r_{\min})r)T_{n_0}^{(\ell)}$ , where  $T_{n_0}^{(\ell)}$  is the tunneling amplitude. The definition of  $k_n(r_{\min}) = \sqrt{2\mu/h^2 E - W_{nm}^{(\ell)}(r_{\min})} > 0$  involves only diagonal elements of the coupling matrix, assuming that the off-diagonal matrix elements tend to be zero (e.g., Refs. [28,29]). We recall that  $W_{nm}^{(\ell)}(r) =$

$\frac{2\mu}{h^2}[V^{(\ell)}(r)\delta_{nm} + V_{nm}(r)]$  at  $r > r_{\min}$ , and the constant valued matrix  $W_{nm} = W_{nm}^{(\ell)}(r_{\min})$  at  $r \leq r_{\min}$ . Here,  $V^{(\ell)}(r) = \frac{Z_p Z_T e^2}{r} + V_N^{(0)}(r) + \frac{\hbar^2 \ell(\ell+1)}{2\mu r^2} + \epsilon_n$  is the potential energy without the coupling. Furthermore,  $V_{nm}(r)$  are elements of the coupling matrix,  $\mu$  is the reduced mass,  $Z_p$  and  $Z_T$  are the Coulomb charges of projectile and target ions,  $\ell$  is the orbital angular momentum, and  $\epsilon_n$  is the excitation energy of the  $n$ th entrance channel or the entrance threshold energy  $E = \epsilon_n$  at  $n = 1, \dots, N$ .

It is important to stress that at  $r_{\min}$ , the distance between two nuclei becomes so small that the off-diagonal matrix elements  $W_{m' \ell}^{(\ell)}(r_{\min})$  are usually not zero. As addressed in Refs. [30,31], there can be sudden noncontinuous changes at the left boundary conditions, and this will distort the total wave function inside the barrier.

To treat properly this problem, at the left boundary we adopt the linear transformation method [26,27]. Namely, at  $r \leq r_{\min}$ , when the off-diagonal matrix elements have been taken into account, the modified solutions of the CC equations  $\tilde{\psi}_{n_0}^{(\ell)}(r)$  consist of the linear independent solutions  $\phi_{nm}^{(\ell)}(r)$ , i.e.,  $\tilde{\psi}_{n_0}^{(\ell)}(r) = \sum_{m=1}^{M_o} \phi_{nm}^{(\ell)}(r) \tilde{T}_{m_0}^{(\ell)}$ . In this case the linear independent matrix solution can be obtained by considering the transformation  $\phi_{nm}(r) = A_{nm} y_m(r)$ , where  $y_m(r)$  are solutions of the uncoupled equations

$$y_m''(r) + K_m^2 y_m(r) = 0, \quad K_m^2 = (2\mu/\hbar^2)E - \tilde{W}_{mm}. \quad (1)$$

Here,  $\mathbf{A}$  and  $\tilde{\mathbf{W}}$  are the matrix of eigenvectors and the diagonal matrix of eigenvalues of the eigenvalue problem, respectively. In short, we diagonalize the coupling matrix  $\mathbf{A}^{-1} \mathbf{W} \mathbf{A} = \tilde{\mathbf{W}}$ . For the open channels with  $K_m^2 > 0$ ,  $y_m(r) = \exp(-iK_m r)/\sqrt{K_m}$  at  $m = 1, \dots, M_o \leq N$ . The partial fusion probability  $P_{n_0}^{(\ell)} = \sum_{m=1}^{M_o} |\tilde{T}_{m_0}^{(\ell)}|^2 \neq \sum_{m=1}^{M_o} |T_{m_0}^{(\ell)}|^2$  is given by

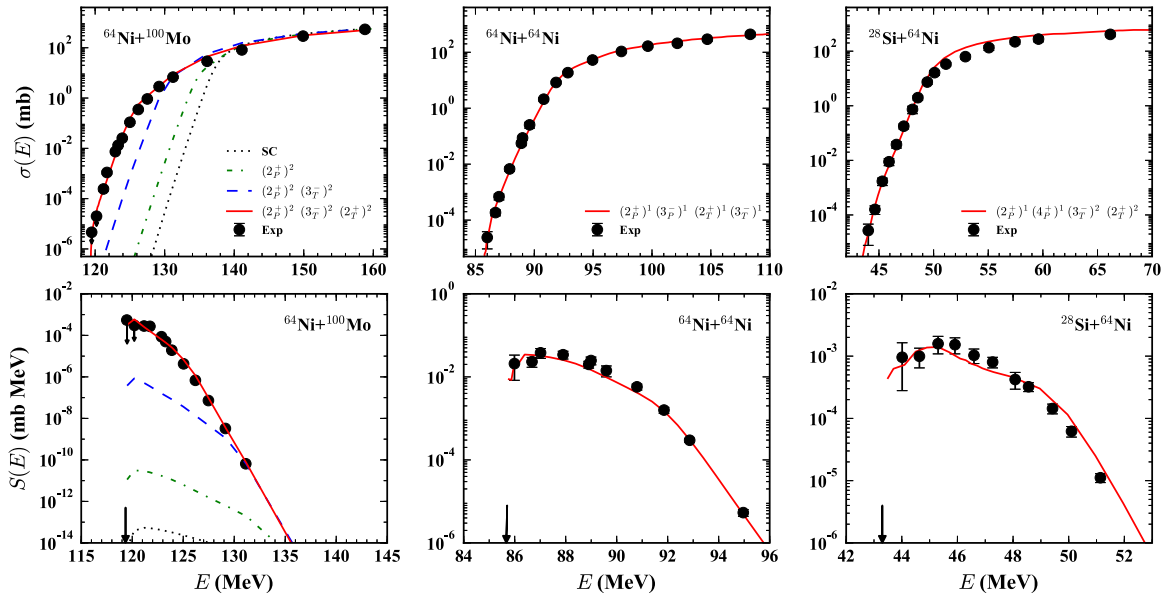


FIG. 1. The fusion cross sections  $\sigma(E)$  and the astrophysical  $S(E)$  factor for  $^{64}\text{Ni} + ^{100}\text{Mo}$ ,  $^{64}\text{Ni} + ^{64}\text{Ni}$ , and  $^{28}\text{Si} + ^{64}\text{Ni}$  reaction systems. Different curves denote the CC calculations with different sets of collective vibrations, indicated by the legends; the SC means a single-channel calculation (without coupling). The experimental data (solid circles) are taken from Refs. [14], [17], and [16], respectively. The black arrows indicate the potential pocket minimum  $V_p$ .

summing over all open exit channels at  $r \leq r_{\min}$ . We stress that the number of open channels after and before the diagonalization of the coupling matrix will be different. At  $r \geq r_{\max}$  the asymptotic solutions are given in terms of the normalized Coulomb functions with the wave number  $k_n = \sqrt{\frac{2\mu}{\hbar^2}(E - \epsilon_n)} > 0$  in the entrance  $n_o$  and the right exit  $n$  open channels  $n_o, n = 1, \dots, N_o \leq N$  and the reflection amplitudes  $\tilde{R}_{m_o}^{(\ell)}$  [27].

### III. RESULTS AND DISCUSSION

To illuminate all the cons and pros of our approach we reexamine  $^{64}\text{Ni} + ^{100}\text{Mo}$ ,  $^{64}\text{Ni} + ^{64}\text{Ni}$ , and  $^{28}\text{Si} + ^{64}\text{Ni}$  reactions. To this aim we analyze the fusion cross sections  $\sigma = \sigma_{\text{fus}}(E) = \sum_{\ell=0}^{\ell_{\max}} \sigma_{\ell}(E) = \frac{\pi}{k_{n_o}^2} \sum_{\ell=0}^{\ell_{\max}} (2\ell + 1) P_{n_o}^{(\ell)}(E)$  and the astrophysical  $S$  factor (see Fig. 1), while  $\sigma(E) = 2 \sum_{\ell=\text{even}}^{\ell_{\max}} \sigma_{\ell}(E)$  for the fusion of two identical nuclei  $^{64}\text{Ni}$ . Our results have been obtained with the aid of the KANTBP code, developed by means of the finite element method (see for details Refs. [32–36]) for the set  $N = 1 + N_{\text{coupl}}$  of CC equations with the improved IWBC from the corresponding ground states  $|n_o - 1 = 0\rangle$ . The number of all channels,  $N_{\text{coupl}}$ , depends on the chosen reaction. It is noteworthy that, using the program KANTBP, the sum of tunneling and reflection probabilities  $\sum_{m=1}^{M_o} |\tilde{T}_{mn_o}^{(\ell)}|^2 + \sum_{n=1}^{N_o} |\tilde{R}_{m_o}^{(\ell)}|^2 - 1 \simeq 10^{-10}$ . Therefore, it is the stringiest test of the validity of our calculations.

The coupling radius parameter for the collective vibrations is set to be 1.2 fm for all the cases in this study [26]. Note that the value of  $\ell_{\max}$  is restricted by the constraint on the incident energy values  $E$  in the entrance channel:  $E = V^{(\ell)}(r_{\min})$ , where  $V^{(\ell)}(r_{\min})$  is the potential minimum, and  $\ell = 0, \dots, \ell_{\max}$ . The values of  $\eta_0$  used for scaling the astrophysical factor  $S(E) = E\sigma_{\text{fus}}(E) \exp(2\pi(\eta - \eta_0))$  for the above three reactions are 105.74, 75.23, and 41.25, respectively;  $\eta$  is the Sommerfeld parameter. The adopted structure properties (including excitation energies, and deformation parameters for the collective states) are taken from Refs. [37,38]. For  $^{64}\text{Ni}$  and  $^{100}\text{Mo}$ , the structure inputs are the same as those listed in Table I of Ref. [26]. For  $^{28}\text{Si}$  the static deformation  $\beta_2 = -0.407$  and the rotational state  $E_{2^+} = 1.780$  MeV are adopted, while for  $^{12}\text{C}$ , the rotational coupling with deformation  $\beta_2 = 0.57$  [24] and the excitation  $E_{2^+} = 4.439$  MeV are adopted. The potential parameters in this study are obtained by fitting the experimental fusion data at the whole energy

TABLE I. Woods-Saxon potential parameters  $V_0$  (MeV),  $a_0$  (fm), and  $R_0$  (fm) for  $^{64}\text{Ni} + ^{100}\text{Mo}$ ,  $^{64}\text{Ni} + ^{64}\text{Ni}$ , and  $^{28}\text{Si} + ^{64}\text{Ni}$  reaction systems. The potential barrier  $V_B$  and the minimum of the potential pocket  $V_P$  are also listed.

	$^{64}\text{Ni} + ^{100}\text{Mo}$	$^{64}\text{Ni} + ^{64}\text{Ni}$	$^{28}\text{Si} + ^{64}\text{Ni}$
$V_0$ (MeV)	79.938	65.829	53.529
$a_0$ (fm)	0.686	0.801	0.944
$R_0$ (fm)	10.190	9.239	7.790
$V_B$ (MeV)	136.993	96.389	51.946
$V_P$ (MeV)	119.344	85.699	43.298

region with the CC calculations and the simple WS potential (see Table I). For the reactions  $^{64}\text{Ni} + ^{64}\text{Ni}$  and  $^{28}\text{Si} + ^{64}\text{Ni}$ , the large diffuseness parameters  $a_0$  are obtained (see also Ref. [39]), while for the reaction  $^{64}\text{Ni} + ^{100}\text{Mo}$  the value of the parameter  $a_0$  is normal. It should be noted, however, that the fitted parameters are sensitive to the considered couplings. For example, various couplings (e.g., the transfer or the decoherence effect that are not considered) may affect the values of the diffuseness parameter in the considered cases.

There is a remarkable agreement between our calculations and available experimental data for the fusion cross sections and  $S$  factors (see Fig. 1). Note that all  $S$  factors of these reactions have maxima. To explore the general reason for the hindrance and the maximum of the  $S$  factor, we consider also the results for different combinations of the collective vibrations for  $^{64}\text{Ni} + ^{100}\text{Mo}$  (see Fig. 1). All calculations for various numbers of coupled channels demonstrate as well the maximum for the  $S$  factor, including the single-channel (SC) case when all  $V_{nm}(r) \equiv 0$  (i.e., without couplings). We observe that the energies, where the hindrance and the maximum of the  $S$  factor take place, are close to the potential pocket minimum  $V_P$  for different couplings.

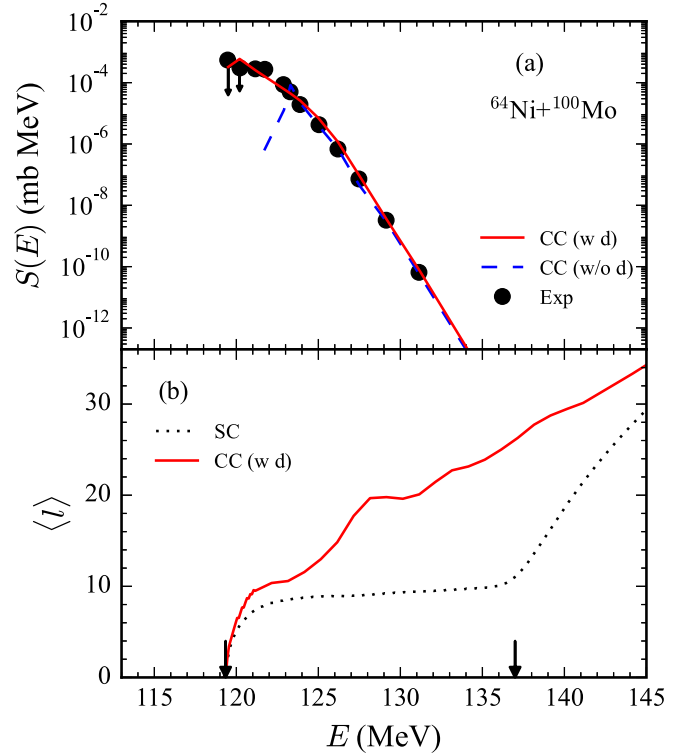


FIG. 2. The astrophysical  $S(E)$  factor and the mean orbital momentum ( $\ell$ ) for the reaction  $^{64}\text{Ni} + ^{100}\text{Mo}$ . (a) The results of the CC calculations with the diagonalization (solid line) and without the diagonalization (dashed line) are compared with the experimental data (solid circles) (see text for details). (b) The mean orbital momentum ( $\ell$ ) for the single channel (without coupling, dotted line) and for the full coupling (solid line) with the diagonalization procedure. The arrows indicate the position of the potential barrier  $V_B$  and the pocket minimum energy  $V_P$ .

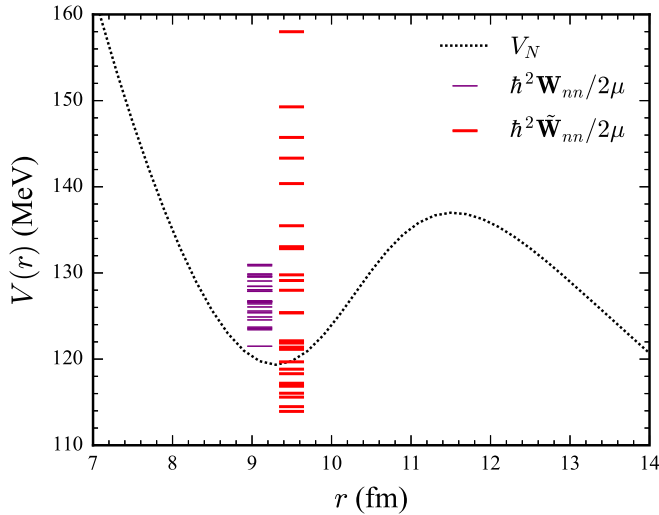


FIG. 3. The potential  $V(r)$  (dotted line), diagonal matrix elements of the coupled matrix  $\hbar^2 \mathbf{W}_{nn}(r_{\min})/2\mu$  (thin solid lines), and eigenvalues  $\hbar^2 \tilde{\mathbf{W}}_{nn}(r_{\min})/2\mu$  (thick solid lines) for the case of  $^{64}\text{Ni} + ^{100}\text{Mo}$ . See text for details.

Although the importance of the potential pocket minimum in the CC calculations was already noticed in Refs. [18,23,40,41], agreement between experimental data and the results of calculations was not reached. In most of these studies the repulsive core inside the shallow potential pocket was suggested as one of the reasons for the hindrance phenomenon. To find out why the hindrance and the maximum of the  $S$  factor happen always near  $V_p$ , we compare the CC results without and with the diagonalization for  $^{64}\text{Ni} + ^{100}\text{Mo}$  [see Fig. 2(a)]. It appears that the correct treatment of the left boundary is one of the decisive factors that allows a good agreement to be reached with the experiment, using the simple WS potential.

To gain further insight into the details of the hindrance phenomenon, we compare the mean angular momentum  $\langle \ell \rangle = \sum_{\ell=0}^{\ell_{\max}} \ell \sigma_{\ell}(E)/\sigma(E)$  (see also Ref. [42]) for the complete calculations and without coupling [see Fig. 2(b)]. Note that when  $E \rightarrow V_p$ , the  $\langle \ell \rangle$  decreases to zero quickly if there is the constraint on the energy for both cases. In this case, the energy is too small, and only the  $s$ -wave partial contribution determines the cross section. It seems that, to obtain a good agreement with the experimental data, the constraint is important as well [compare Figs. 2(a) and 2(b)]. At  $E > V_p$  there are many coupled channels in the complete calculations, and, consequently, the barrier has a certain kind of distribution, which obscures the barrier position.

To elucidate further the basic mechanism of the hindrance factor in our calculations, we compare the potential energy  $V(r)$  (without coupling), the diagonal elements  $\hbar^2 \mathbf{W}_{nn}/2\mu$  of the coupled matrix, and the threshold energies  $\hbar^2 \tilde{\mathbf{W}}_{nn}/2\mu$  at the left boundary (see Fig. 3). As it is seen, the threshold energies  $\hbar^2 \tilde{\mathbf{W}}_{nn}/2\mu$  spread much wider than the diagonal elements  $\hbar^2 \mathbf{W}_{nn}/2\mu$  of the coupled matrix. In particular, the minimum threshold energy of  $\hbar^2 \tilde{\mathbf{W}}_{11}/2\mu$  is obviously much lower than  $V_p$ . In other words, in contrast to the conventional

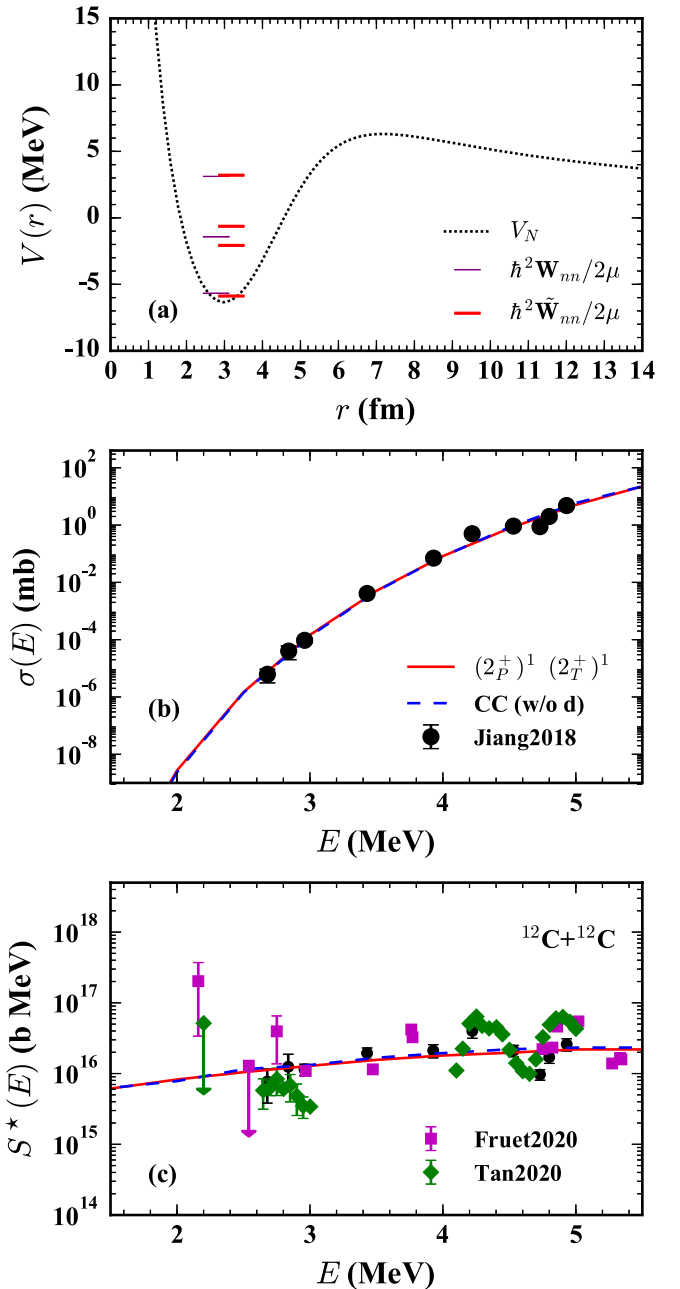


FIG. 4. (a) Similar to Fig. 3 for the case of  $^{12}\text{C} + ^{12}\text{C}$ . (b) The results for the fusion cross sections  $\sigma(E)$  with the diagonalization (solid line) and without the diagonalization (dashed line). (c) The results for the  $S^*(E)$  factor with the diagonalization (solid line) and without the diagonalization (dashed line). The experimental data labeled as Jiang2018, Tan2020, and Fruet2020 are taken from Refs. [8], [10], [11], respectively. All results are obtained with the indicated collective vibrations.

CC calculations, in our approach the distribution of open channels is wider.

It appears that the experimental fusion cross section can be reproduced well only under certain physical couplings. For these reactions, the entanglement between the states at the left boundary is changed through the diagonalization procedure.

On the other hand, in the CC calculations, when the incident energy  $E < V_p = V^{(\ell=0)}(r_{\min})$ , the tunneling is absent. It is due the fact that the ingoing flux will be zero [23,28,40]. Thus, when the incident energy gradually approaches the bottom of the potential pocket minimum, the fusion hindrance occurs naturally.

Let us turn to the most important fusion reaction  $^{12}\text{C} + ^{12}\text{C}$  in nuclear astrophysics within our approach. We recall that the carbon fusion plays a significant role in the burning of massive stars, ignition of the type Ia supernova explosion, and superbursts of binary systems or neutron stars [2]. It remains an open problem whether the fusion hindrance does, indeed, occur in this reaction, which is closely related to the astrophysical reaction rate [8,13].

As above, we fit the experimental fusion cross section [8] with the aid of the WS potential:  $V_0 = 30.334$  MeV,  $R_0 = 4.113$  fm, and  $a_0 = 0.883$  fm. In addition, we consider the quadrupole excitations. In this case the fusion cross section is defined as  $\sigma(E) = 2 \sum_{\ell=\text{even}}^{\ell_{\max}} \sigma_{\ell}(E)$ . For the carbon fusion, we adopt the commonly used definition  $S^*(E) = \sigma(E)E \exp(87.21/\sqrt{E} + 0.46E)$  [10,12]. The results of calculations with and without the diagonalization demonstrate a good agreement with the general trend of experimental fusion data [8,10]. In contrast to the results shown in Fig. 1, where the  $S(E)$  factor drops at the low energy tail region evidently, the  $S^*(E)$  factor evolves smoothly with the decreasing energy. It should be noted that the trend of the  $S^*(E)$  factor over the energy  $E$  is different from that for the  $S(E)$  factor. At the low energy region,  $S^*(E)$  is lower than that of  $S(E)$ . And for the  $S^*(E)$  factor, the calculations indicate that there are no clear decrease and maximum for this system at low energies. Note that our results are similar to those of the CC theory with the M3Y+repulsive core potential in Ref. [24].

In our calculations, based on the WS potential, the reason for the steady trend can be traced from Fig. 4(a). The threshold energies after the diagonalization change modestly in comparison with those without the diagonalization. The bottom of the potential pocket is about  $-7$  MeV, which is far from the incident energy region of interest (about 1.5–3 MeV). Therefore, the hindrance feature is not so obvious as that seen in Fig. 1. In the former case the  $S^*$  factor changes slowly below the potential barrier.

Surprisingly, we find that our results are supported by the empirical trends, discussed for the hindrance factor in Ref. [43]. Indeed, our results for the medium nuclei manifest the hindrance factor for a system with  $Z_1 Z_2 \sqrt{\mu} \geq 2000$ . However, for the lightest system with  $Z_1 Z_2 \sqrt{\mu} \leq 200$  the logarithmic slopes of the  $S^*(E)$  factor exhibit resistance to the increasing tendency with the energy. In our approach the variation of the coupling strength of the left exit channels is the basic mechanism responsible for the observed phenomenon. In other words, the degree of the strength

controls the number of open channels, contributing to the reaction.

#### IV. SUMMARY

The deep subbarrier heavy-ion fusion hindrance phenomenon and the behavior of the astrophysical  $S$  factor for  $^{64}\text{Ni} + ^{100}\text{Mo}$ ,  $^{64}\text{Ni} + ^{64}\text{Ni}$ , and  $^{28}\text{Si} + ^{64}\text{Ni}$  reactions are analyzed by solving the CC equations with the improved IWBC. This approach was developed in Refs. [26,27] based on the finite element method KANTBP code [32–36]. The obtained results reproduce remarkably well the experimental data with the aid of the simple WS potential. It is found that the calculated  $S$  factors with different kinds of collective excitations have maxima for the considered reactions. The knowledge of the potential minimum energy  $V_p$  and the improved IWBC are crucially important for the correct interpretation of the fusion cross section in the conventional CC calculations based on the sudden approximation. The general trend of the directly measured fusion data for the reaction  $^{12}\text{C} + ^{12}\text{C}$  [8,10] is described as well. It is found that the  $S^*$  factor drops gently at energies under the Coulomb barrier, and the results have not shown pronounced maximum of the  $S^*$  factor for this system. We hope that further experiments at even lower energies could finally reveal the “mystery of the hindrance phenomenon” as a function of the mass number. From our point of view it is determined by the number of coupled channels at the correct treatment of the left boundary conditions for different combinations of the colliding nuclei.

#### ACKNOWLEDGMENTS

The work of P.W.W., C.J.L., and H.M.J. is supported by the National Natural Science Foundation of China (Grants No. 11635015, No. 11805280, No. U1867212, and No. 11961131012), the National Key R&D Program of China (Contract No. 2018YFA0404404), the Continuous Basic Scientific Research Project (No. WDJC-2019-13), and the Leading Innovation Project under Grants No. LC192209000701 and No. LC202309000201. The present research benefited from computational resources of the HybriLIT heterogeneous platform of the JINR. This work was partially supported by the Polish-French COPIN collaboration of the project 04-113, the Bogoliubov-Infeld and the Hulubei-Meshcheryakov JINR programs, the grant RFBR and MECSS 20-51-44001, the grant of Ministry of Education and Science of the Russian Federation 075-10-2020-117, the grant RFBR 17-52-45037, the RUDN University Strategic Academic Leadership Program, the grant of Plenipotentiary of the Republic of Kazakhstan in JINR, and the grant of Foundation of Science and Technology of Mongolia SST\_18/2018.

[1] G. Montagnoli and A. M. Stefanini, *Eur. Phys. J. A* **53**, 169 (2017).

[2] B. B. Back, H. Esbensen, C. L. Jiang, and K. E. Rehm, *Rev. Mod. Phys.* **86**, 317 (2014).

- [3] C. J. Lin, *Heavy-Ion Nuclear Reactions* (Harbin Engineering University Press, Harbin, China, 2015).
- [4] L. Yang, C. J. Lin, H. M. Jia, D. X. Wang, N. R. Ma, L. J. Sun, F. Yang, X. X. Xu, Z. D. Wu, H. Q. Zhang, and Z. H. Liu, *Phys. Rev. Lett.* **119**, 042503 (2017).
- [5] H. M. Jia, C. J. Lin, L. Yang, X. X. Xu, N. R. Ma, L. J. Sun, F. Yang, Z. D. Wu, H. Q. Zhang, Z. H. Liu, and D. X. Wang, *Phys. Lett. B* **755**, 43 (2016).
- [6] A. K. Nasirov, B. M. Kayumov, G. Mandaglio, G. Giardina, K. Kim, and Y. Kim, *Eur. Phys. J. A* **55**, 29 (2019).
- [7] C. L. Jiang, H. Esbensen, K. E. Rehm, B. B. Back, R. V. F. Janssens, J. A. Caggiano, P. Collon, J. Greene, A. M. Heinz, D. J. Henderson, I. Nishinaka, T. O. Pennington, and D. Seweryniak, *Phys. Rev. Lett.* **89**, 052701 (2002).
- [8] C. L. Jiang, D. Santiago-Gonzalez, S. Almaraz-Calderon, K. E. Rehm, B. B. Back, K. Auranen, M. L. Avila, A. D. Ayangeakaa, S. Bottoni, M. P. Carpenter, C. Dickerson, B. DiGiovine, J. P. Greene, C. R. Hoffman, R. V. F. Janssens, B. P. Kay, S. A. Kuvin, T. Lauritsen, R. C. Pardo, J. Sethi, D. Seweryniak, R. Talwar, C. Ugalde, S. Zhu, D. Bourgin, S. Courtin, F. Haas, M. Heine, G. Fruet, D. Montanari, D. G. Jenkins, L. Morris, A. Lefebvre-Schuhl, M. Alcorta, X. Fang, X. D. Tang, B. Bucher, C. M. Deibel, and S. T. Marley, *Phys. Rev. C* **97**, 012801(R) (2018).
- [9] A. Tumino, C. Spitaleri, M. La Cognata, S. Cherubini, G. L. Guardo, M. Gulino, S. Hayakawa, I. Indelicato, L. Lamia, H. Petruscu, R. G. Pizzone, S. M. R. Puglia, G. G. Rapisarda, S. Romano, M. L. Sergi, R. Sparta, and L. Trache, *Nature* **557**, 687 (2018).
- [10] W. P. Tan, A. Boeltzig, C. Dulal, R. J. deBoer, B. Frenzt, S. Henderson, K. B. Howard, R. Kelmar, J. J. Kolata, J. Long, K. T. Macon, S. Moylan, G. F. Peaslee, M. Renaud, C. Seymour, G. Seymour, B. Vande Kolk, M. Wiescher, E. F. Aguilera, P. Amador-Valenzuela, D. Lizcano, and E. Martinez-Quiroz, *Phys. Rev. Lett.* **124**, 192702 (2020).
- [11] G. Fruet, S. Courtin, M. Heine, D. G. Jenkins, P. Adsley, A. Brown, R. Canavan, W. N. Catford, E. Charon, D. Curien, S. Della Negra, J. Duprat, F. Hammache, J. Lesrel, G. Lotay, A. Meyer, D. Montanari, L. Morris, M. Moukaddam, J. Nippert, Z. Podolyák, P. H. Regan, I. Ribaud, M. Richer, M. Rudigier, R. Shearman, N. de Séréville, and C. Stodel, *Phys. Rev. Lett.* **124**, 192701 (2020).
- [12] Y. J. Li, X. Fang, B. Bucher, K. A. Li, L. H. Ru, and X. D. Tang, *Chin. Phys. C* **44**, 115001 (2020).
- [13] C. Beck, A. M. Mukhamedzhanov, and X. Tang, *Eur. Phys. J. A* **56**, 87 (2020).
- [14] C. L. Jiang, K. E. Rehm, H. Esbensen, R. V. F. Janssens, B. B. Back, C. N. Davids, J. P. Greene, D. J. Henderson, C. J. Lister, R. C. Pardo, T. Pennington, D. Peterson, D. Seweryniak, B. Shumard, S. Sinha, X. D. Tang, I. Tanihata, S. Zhu, P. Collon, S. Kurtz, and M. Paul, *Phys. Rev. C* **71**, 044613 (2005).
- [15] M. Dasgupta, D. J. Hinde, A. Diaz-Torres, B. Bouriquet, C. I. Low, G. J. Milburn, and J. O. Newton, *Phys. Rev. Lett.* **99**, 192701 (2007).
- [16] C. L. Jiang, B. B. Back, H. Esbensen, R. V. F. Janssens, Ş. Mişicu, K. E. Rehm, P. Collon, C. N. Davids, J. Greene, D. J. Henderson, L. Jisonna, S. Kurtz, C. J. Lister, M. Notani, M. Paul, R. Pardo, D. Peterson, D. Seweryniak, B. Shumard, X. D. Tang, I. Tanihata, X. Wang, and S. Zhu, *Phys. Lett. B* **640**, 18 (2006).
- [17] C. L. Jiang, K. E. Rehm, R. V. F. Janssens, H. Esbensen, I. Ahmad, B. B. Back, P. Collon, C. N. Davids, J. P. Greene, D. J. Henderson, G. Mukherjee, R. C. Pardo, M. Paul, T. O. Pennington, D. Seweryniak, S. Sinha, and Z. Zhou, *Phys. Rev. Lett.* **93**, 012701 (2004).
- [18] Ş. Mişicu and H. Esbensen, *Phys. Rev. Lett.* **96**, 112701 (2006).
- [19] K. Hagino, A. B. Balantekin, N. W. Lwin, and Ei Shwe Zin Thein, *Phys. Rev. C* **97**, 034623 (2018).
- [20] T. Ichikawa, K. Hagino, and A. Iwamoto, *Phys. Rev. Lett.* **103**, 202701 (2009).
- [21] V. V. Sargsyan, G. G. Adamian, N. V. Antonenko, and H. Lenske, *Eur. Phys. J. A* **56**, 19 (2020).
- [22] C. Simenel, A. S. Umar, K. Godbey, M. Dasgupta, and D. J. Hinde, *Phys. Rev. C* **95**, 031601(R) (2017).
- [23] Ş. Mişicu and H. Esbensen, *Phys. Rev. C* **75**, 034606 (2007).
- [24] H. Esbensen, X. Tang, and C. L. Jiang, *Phys. Rev. C* **84**, 064613 (2011).
- [25] T. Ichikawa, K. Hagino, and A. Iwamoto, *Phys. Rev. C* **75**, 064612 (2007).
- [26] P. W. Wen, O. Chuluunbaatar, A. A. Gusev, R. G. Nazmitdinov, A. K. Nasirov, S. I. Vinitzky, C. J. Lin, and H. M. Jia, *Phys. Rev. C* **101**, 014618 (2020).
- [27] S. I. Vinitzky, P. W. Wen, A. A. Gusev, O. Chuluunbaatar, R. G. Nazmitdinov, A. K. Nasirov, C. J. Lin, H. M. Jia, and A. Góźdź, *Acta Phys. Pol. B Proc. Suppl.* **13**, 549 (2020).
- [28] K. Hagino, N. Rowley, and A. T. Kruppa, *Comput. Phys. Commun.* **123**, 143 (1999).
- [29] K. Hagino and N. Takigawa, *Prog. Theor. Phys.* **128**, 1061 (2012).
- [30] V. I. Zagrebaev and V. V. Samarin, *Phys. At. Nucl.* **67**, 1462 (2004).
- [31] V. V. Samarin and V. I. Zagrebaev, *Nucl. Phys. A* **734**, E9 (2004).
- [32] O. Chuluunbaatar, A. A. Gusev, A. G. Abrashkevich, A. Amaya-Tapia, M. S. Kaschiev, S. Y. Larsen, and S. I. Vinitzky, *Comput. Phys. Commun.* **177**, 649 (2007).
- [33] O. Chuluunbaatar, A. A. Gusev, S. I. Vinitzky, and A. G. Abrashkevich, *Comput. Phys. Commun.* **179**, 685 (2008).
- [34] A. A. Gusev, O. Chuluunbaatar, S. I. Vinitzky, and A. G. Abrashkevich, *Comput. Phys. Commun.* **185**, 3341 (2014).
- [35] A. A. Gusev, O. Chuluunbaatar, S. I. Vinitzky, and A. G. Abrashkevich, *Math. Mod. Geom.* **3**, 22 (2015).
- [36] G. Chuluunbaatar, A. A. Gusev, O. Chuluunbaatar, S. I. Vinitzky, and L. Le Hai, *EPJ Web Conf.* **226**, 02008 (2020).
- [37] S. Raman, C. W. Nestor, and P. Tikkanen, *At. Data Nucl. Data Tables* **78**, 1 (2001).
- [38] T. Kibédi and R. H. Spear, *At. Data Nucl. Data Tables* **80**, 35 (2002).
- [39] K. Hagino, N. Rowley, and M. Dasgupta, *Phys. Rev. C* **67**, 054603 (2003).
- [40] G. Montagnoli, A. M. Stefanini, H. Esbensen, C. L. Jiang, L. Corradi, S. Courtin, E. Fioretto, A. Goasduff, J. Grebosz, F. Haas, M. Mazzocco, C. Michelagnoli, T. Mijatovic, D. Montanari, C. Parascandolo, K. E. Rehm, F. Scarlassara, S. Szilner, X. D. Tang, and C. A. Ur, *Phys. Rev. C* **87**, 014611 (2013).
- [41] C. H. Dasso and G. Pollarolo, *Phys. Rev. C* **68**, 054604 (2003).
- [42] K. Hagino, N. Takigawa, M. Dasgupta, D. J. Hinde, and J. R. Leigh, *Phys. Rev. C* **55**, 276 (1997).
- [43] C. L. Jiang, B. B. Back, H. Esbensen, R. V. F. Janssens, and K. E. Rehm, *Phys. Rev. C* **73**, 014613 (2006).